



# Geometrical Analysis to Blood Flow Across Tapered-Non Tapered Arteries by the Use of Various Advanced Flow Parameters

A. N. M. Rezaul Karim<sup>\*1</sup> , Mohammed Nizam Uddin<sup>2</sup>  and Mahmuda Akter<sup>2</sup> 

<sup>1</sup>Department of Computer Science & Engineering, International Islamic University Chittagong, Kumira, Sitakunda, Chittagong 4318, Bangladesh

<sup>2</sup>Department of Applied Mathematics, Noakhali Science and Technology University, Noakhali, Bangladesh

\*Corresponding author: zakianaser@yahoo.com

Received: December 31, 2020

Accepted: January 19, 2021

Published: March 31, 2021

**Abstract.** The study of Arterial blood flow is a fascinating topic as arterial disease is responsible of death in many nations. This paper investigated the conduct of blood flow across a tapered artery with stenosis. This study has been simply explained by the use of a mathematical model that is appropriate. The graphical representations were created to support the results of the study. For various values of tapering angle, it is discovered that wall shear stress enhance when a peak is reached, then decreases. We also found that the velocity of the blood flow reduces with radius and also for distinct values of tapering angle. It is also evidenced that the blood flow rate reduces as the radius and tapering angle increase.

**Keywords.** Aortic aneurysm; Perturbation solution; Pressure contours; Reynolds number (Re); Weissenbergnumber(Wi); Hartmannnumber(Ha), Wall Shear Stress

**Mathematics Subject Classification (2020).** 35B30

Copyright © 2021 A. N. M. Rezaul Karim, Mohammed Nizam Uddin and Mahmuda Akter. *This is an open access article distributed under the Creative Commons Attribution License, which permits unrestricted use, distribution, and reproduction in any medium, provided the original work is properly cited.*

## 1. Introduction

### 1.1 Blood

The heart is in charge of pumping blood and supplying oxygen and nutrients across the body as part of the circulatory system. The fluid that carries away carbon dioxide and other waste

products while providing oxygen and nutrients to cells is known as blood. A human body contains about 5 liters of blood (more than a gallon) [19]. The heart [43] drives blood to various parts of the body as a carrier liquid and blood comes back to the heart to repeat the cycle. At the same time, Blood is a tissue because it is a group of identical particular cells that serve specific functions. These cells are floating in a liquid matrix (plasma); which is responsible for the fluidity of the blood. When blood flow stops, very sensitive cells die within minutes due to the effects of the hostile environment.

## 1.2 Blood Components

Plasma, red blood cells (RBC), white blood cells (WBC), and platelets are the four primary components of a blood sample [37, 44]. The golden-yellow liquid portion of blood is known as plasma. Proteins, glucose, ions, hormones, and gases make up 10% of plasma's dissolved products. It functions as a buffer, maintaining the pH close to 7.4. Plasma accounts for around 54% of blood volume, while cells and fragments account for 46% [39]. Hemoglobin is a special protein found in red blood cells that assists in the transportation of oxygen from the lungs to the entire body, as well as the return of Carbon dioxide is transported from the body to the lungs, where it is exhaled. The diameter of red cells is approximately 7.8  $\mu$ m (1  $\mu$ m = 0.000039 inch). Just about 1% of our blood is made up of white blood cells, but they have a huge effect. Leukocytes are the term for white blood cells. They safeguard us from disease and illness [1]. Platelets are small blood cells that assist in the formation of clots to avoid bleeding [11].

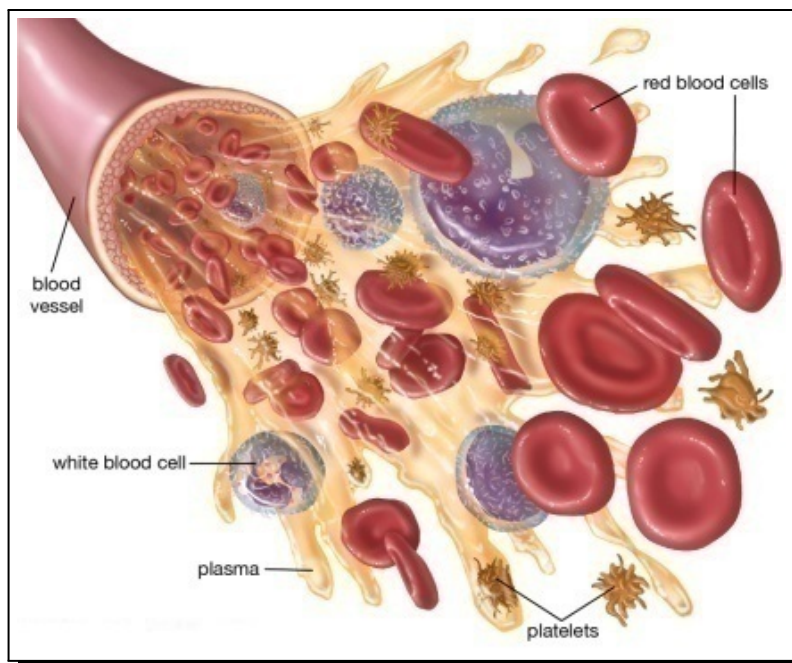


**Figure 1.** Component of blood cell [source: encyclopedia britannica, inc.]

### 1.3 Aortic Aneurysm

The aorta, which is responsible for transporting oxygen-rich blood from the heart to the entire of the body, is the most significant blood vessel (pipe) inside the body of man. A part of the aorta wall may be damaged or weakened in some cases. As a result of this, it can bulge or swell similar to a balloon which is referred to as aortic aneurysm. Stenosis is a word that applies to any disorder situation in which a blood vessel (an artery), or another tubular organ narrows strangely.

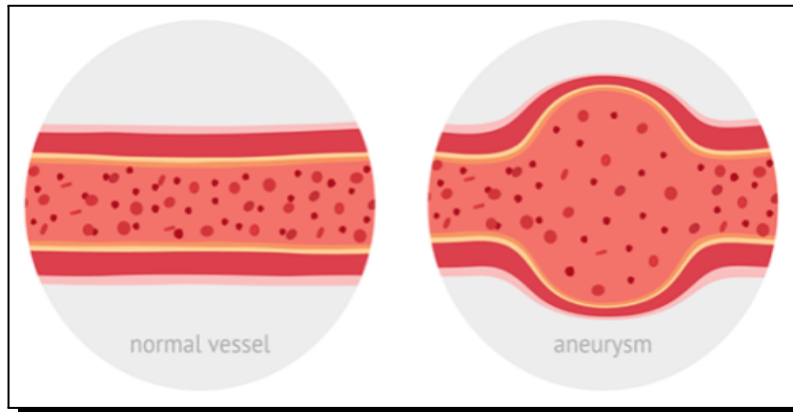


**Figure 2.** Normal vessel vs weakened vessel [source: encyclopedia britannica, inc]

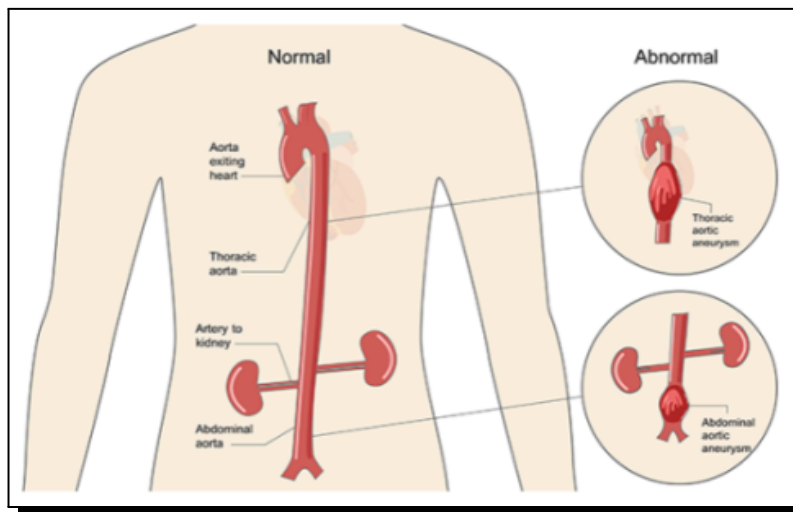


**Figure 3.** Abdominal aortic aneurysm and thoracic aortic aneurysm [source: encyclopedia britannica, inc]

### 1.4 Types of Aortic Aneurysms

There are two types of aneurysms. This bulge is most commonly seen in the lower portion of aorta, which passes across abdomen (tummy); that is known as an aortic aneurysm in the abdomen (AAA). In some cases, the bulge can take place in the upper portion of the aorta that runs across our chest; that is known as thoracic aortic aneurysm [12, 43, 50].

## 1.5 Aortic aneurysm complications

When there is a small aortic aneurysm, it normally causes no complications, but when it becomes too large, it can be fatal. Two types of symptoms may be manifested: (i) Aortic dissection (a tear in its wall of the aorta), (ii) Aortic rupture (the aorta to burst).

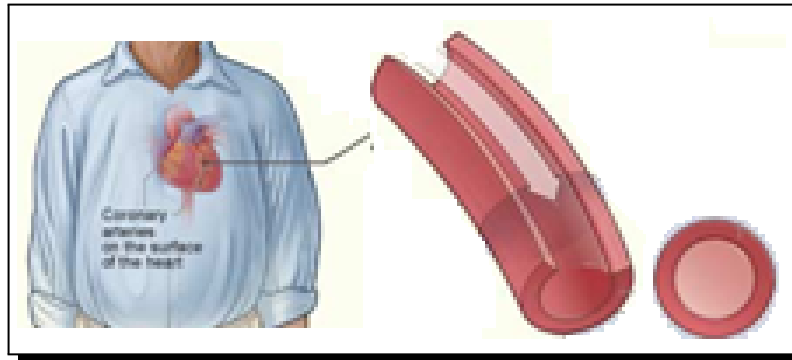


**Figure 4.** Normal blood flow through normal coronary artery [source: encyclopedia britannica, inc]

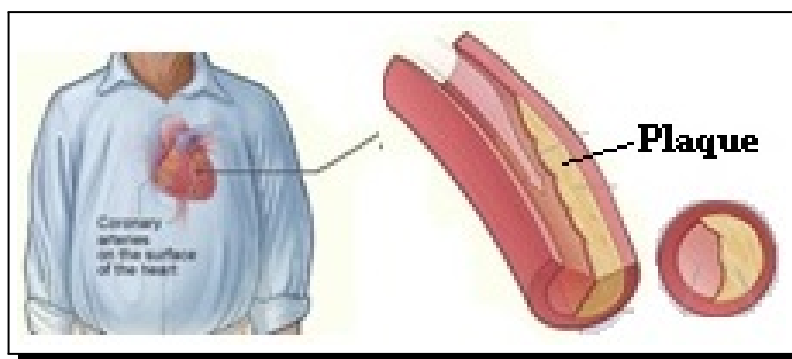


**Figure 5.** Abnormal blood flow through narrowing of coronary artery [source: encyclopedia britannica, inc]

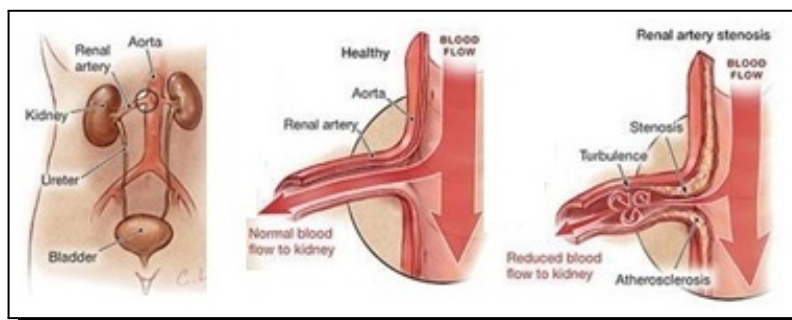


**Figure 6.** Normal vs abnormal blood flow to kidney [source: encyclopedia britannica, inc]

## 1.6

A thoracic aortic aneurysm can manifest itself in a number of ways, chest tightness or discomfort, back pain, hoarseness, cough, shortness of breath are some of the symptoms that may occur.

And An abdominal aortic aneurysm can cause a variety of symptoms: serious abdominal pain or the side of our abdomen, back or groin pain, pulsing sensation around our belly button [19].

### 1.7 Newtonian Fluid versus Non-Newtonian Fluid

Newtonian fluid is characterized as a fluid that follows the rules of Newton's law of viscosity (Example: water, benzene, ethyl alcohol etc). Otherwise it is called Non-Newtonian [15] Fluid (Example: blood, saliva, toothpaste, paint etc.). The viscosity of a fluid is commonly referred to as its thickness (Example: honey with high viscosity and water with low viscosity).

## 2. Literature Review

Tapering is an important factor of the mammalian arterial system. Several studies have been conducted on blood flow in arteries theoretically, experimentally, clinically and numerically [7, 12, 29, 33, 37]. The intricate anatomy of arteries (such as stretching, bifurcation, stenosis, and so on) is also a significant factor that affects local hemodynamics. Localized arterial narrowing is a symptom of arteriosclerosis (or stenosis). Local hemodynamics can be affected by stenosis. Simultaneously, changes in local hemodynamics can result in blood vessel re-narrowing (restenosis). A number of studies have documented their experimental work in rigid stenoses, such as Ahmed [2], and Siouffi et al. [16,47]. The pulsatile flow in flexible stenoses was calculated by Stergiopoulos et al. [30]. Pulsatile flow through axially symmetric smooth rigid stenoses: a numerical analysis. There have been reports of experiments using blood as an incompressible Newtonian fluid [10, 31, 54]. Moreover, Tu and Deville [52] as well as Ishikawa and coworkers [18,21] have considered the non-Newtonian properties of blood. The effect of stenosis morphology has been highlighted by Stroud et al. [48]. Andersson et al. [5] described stenosis as abnormal stenosis on the surface. The effects of the wall's elastic property were studied by Moayeri and Zendehebudi [38]. Chakravarty and Sannigrahi [14] devised a nonlinear mathematical model to examine blood flow features in an artery with multi-stenoses when subjected to whole-body acceleration. Valencia and Villanueva [53] developed a computational model to simulate non-Newtonian blood flow and mass transfer that is not always compatible stenotic arteries, both symmetric and non-symmetric. Bakirtas and Demiray examined the impact of stenosis on solitary waves in arteries [6]. The exponential taper in arteries was studied by Myers and Capper [40]. The effect of precise solution impedance and waveforms of blood flow velocity has been investigated. Sankar explored the pulsatile flow of blood via a catheterized artery [45] assuming a two-fluid model for blood. As a pioneering contribution to the study of the viscoelastic nature of blood shear thinning. Thurston [51] created a one-dimensional flow model based on an expanded Maxwell model. For blood moving into tiny vessels; some researchers [4, 13, 34–36] examined this. There is a layer of erythrocyte-free plasma (Newtonian) neighboring to the vessel wall, as well as a central layer of erythrocyte suspension (non-Newtonian) [17, 22–26].

Cardiovascular infections (such as coronary heart [32] disease, stroke, aneurysm, and stenosis) are regarded as the cause of the largest number of deaths in the world [28]. Cerebral

aneurysm is a form of coronary heart disease. The most common cause of internal bleeding is the rupture of cerebral aneurysms; which is a life-threatening condition that results in mortality and morbidity [20, 27].

### 3. Formulation of the Problem

A circular part of a rigid tube is used to mathematically model the tapered vessel segment with an axially symmetric stenosis.

Let  $(r, \theta, z)$  be the coordinates, with the  $z$ -axis running parallel to the artery's axis and  $r$  and  $\theta$  running parallel to the radial and circumferential directions, correspondingly.

The mathematical model of the artery's geometry (Figures 7 and 8) is as follows:

$$\psi(z) = \begin{cases} R_0 - m(z + d) - \frac{h \cos \phi}{2} \left( 1 + \cos \frac{\pi z}{z_0} \right); & |z| \leq z_0 \\ R_0 - m(z + d); & |z| > z_0 \end{cases} \quad (3.1)$$

where  $\psi(z)$  is the radius of the constricted region's tapered arterial section. In the non-stenotic area,  $R_0$  is the constant radius of the straight artery,  $\phi$  denotes the tapering angle. For tapered arteries,  $h \cos \phi$  is the stenosis height. The half-length of the stenosis is  $z_0$ , and the slope of the tapered vessel is  $m (= \tan \phi)$ . If the blood flow in the stenotic and tapered arterial segment is pulsating, axis symmetric, two-dimensional, and completely formed, the Navier-Stokes equations and the equation of continuity governing the blood flow are written in cylindrical coordinates as

$$\frac{\delta u}{\delta t} + u \frac{\delta u}{\delta z} + v \frac{\delta u}{\delta r} = -\frac{1}{\rho} \frac{\delta p}{\delta z} + \frac{\mu}{\rho} \left( \frac{\delta^2 u}{\delta r^2} + \frac{1}{r} \frac{\delta u}{\delta r} + \frac{\delta^2 u}{\delta z^2} \right), \quad (3.2)$$

$$\frac{\delta v}{\delta t} + u \frac{\delta v}{\delta z} + v \frac{\delta v}{\delta r} = -\frac{1}{\rho} \frac{\delta p}{\delta r} + \frac{\mu}{\rho} \left( \frac{\delta^2 v}{\delta r^2} + \frac{1}{r} \frac{\delta v}{\delta r} + \frac{\delta^2 v}{\delta z^2} - \frac{v}{r^2} \right), \quad (3.3)$$

$$\frac{\delta u}{\delta z} + \frac{1}{r} \frac{\delta(rv)}{\delta r} = 0. \quad (3.4)$$

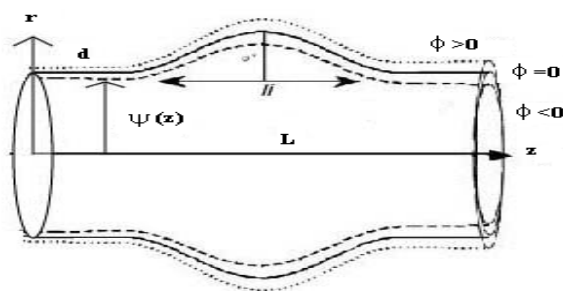


**Figure 7.** Geometry of the artery in longitudinal section

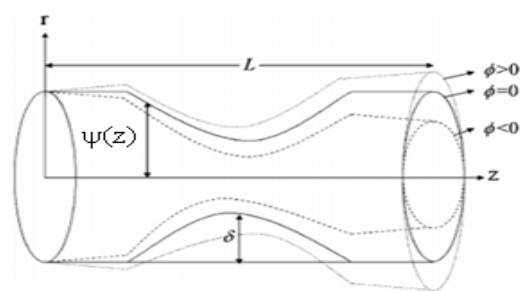


**Figure 8.** Geometry of the axially stenosed tapered artery for different tapered angle

Here,  $u$  and  $v$  stand for the axial and radial velocity components, correspondingly.  $p$  stands for pressure,  $\rho$  is the blood's density, and  $\mu$  symbolize the blood viscosity.

We introduce the following dimensionless variables:

$$r^* = \frac{r}{R_0}, \quad z^* = \frac{z}{R_0}, \quad u^* = \frac{u}{u_0}, \quad v^* = \frac{v}{u_0}, \quad t^* = \frac{t}{T}, \tag{3.5}$$

where  $u_0$  the average velocity is in a period over the inlet section,  $T$  is the pulsating period of the blood flow. We use the stream function vorticity structure of the equations to make solving the governing equations more convenient. In two-dimensional incompressible flow; this form has several advantages over the primitive variable form. Since, it automatically solves the continuity equation. As a result, we begin by introducing the dimensionless stream function  $\psi^*$  and dimensionless vorticity  $\Omega^*$

$$u^* = \frac{1}{r^*} \frac{\delta \psi^*}{\delta r^*}, \quad v^* = -\frac{1}{r^*} \frac{\delta \psi^*}{\delta z^*}, \quad \Omega^* = \frac{\delta v^*}{\delta z^*} - \frac{\delta u^*}{\delta r^*}. \tag{3.6}$$

The stream function and vorticity equations are obtained by removing  $p$  from equations (3.2) and (3.3) and substituting equations (3.5) and (3.6).

$$\frac{\delta^2 \psi}{\delta z^2} + \frac{\delta^2 \psi}{\delta r^2} - \frac{1}{r} \frac{\delta \psi}{\delta r} = -r\Omega. \tag{3.7}$$

Such that

$$\frac{\delta \Omega}{\delta t} + \frac{1}{r} \frac{\delta \psi}{\delta r} \frac{\delta \Omega}{\delta z} - \frac{1}{r} \frac{\delta \psi}{\delta z} \frac{\delta \Omega}{\delta r} = \frac{1}{Re} \left[ \frac{\delta^2 \Omega}{\delta r^2} + \frac{1}{r} \frac{\delta \Omega}{\delta r} + \frac{\delta^2 \Omega}{\delta z^2} - \frac{\Omega}{r^2} \right] - \frac{\Omega}{r^2} \frac{\delta \psi}{\delta z}. \tag{3.8}$$

The following are the steady incompressible tangent hyperbolic fluid equations:

$$\frac{\delta \bar{u}}{\delta \bar{r}} + \frac{\bar{u}}{\bar{r}} + \frac{\delta \bar{w}}{\delta \bar{z}} = 0. \tag{3.9}$$

In both the  $\bar{r}$  and  $\bar{z}$  directions, the velocity components

$$\rho \left( \bar{u} \frac{\delta}{\delta \bar{r}} + \bar{w} \frac{\delta}{\delta \bar{z}} \right) \bar{u} = -\frac{\delta \bar{p}}{\delta \bar{z}} + \frac{1}{\bar{r}} \frac{\delta}{\delta \bar{r}} (\bar{r} \bar{\tau}_{\bar{r}\bar{r}}) + \frac{\delta}{\delta \bar{z}} (\bar{\tau}_{\bar{r}\bar{z}}) - \frac{\bar{\tau}_{00}}{\bar{r}}, \tag{3.10}$$

$$\rho \left( \bar{u} \frac{\delta}{\delta \bar{r}} + \bar{w} \frac{\delta}{\delta \bar{z}} \right) \bar{w} = -\frac{\delta \bar{p}}{\delta \bar{z}} + \frac{1}{\bar{r}} \frac{\delta}{\delta \bar{r}} (\bar{r} \bar{\tau}_{\bar{r}\bar{z}}) + \frac{\delta}{\delta \bar{z}} (\bar{\tau}_{\bar{z}\bar{z}}). \tag{3.11}$$

Blood in the vessel is treated as incomplete and turbulent flow. In both the  $r$  and  $z$  directions, velocity components must be described. For non-Newtonian fluids, the shape of the dimensionless Navier-Stokes equation [3, 9, 41].

$$\psi e \sigma \varepsilon^2 \left( \frac{\partial u}{\partial t} + \varepsilon \left( \sigma u \frac{\partial u}{\partial r} + v \frac{\partial u}{\partial z} \right) \right) = -\frac{\partial p}{\partial r} + \varepsilon^2 \left( \frac{1}{r} \frac{\partial}{\partial r} (r S^{rr}) + \frac{\partial}{\partial z} (S^{rz}) \right), \tag{3.12}$$

$$\psi e \left[ \frac{\partial v}{\partial t} \right] + \psi e \left( \sigma \varepsilon u \frac{\partial v}{\partial r} + \varepsilon v \frac{\partial v}{\partial z} \right) = -\frac{\partial p}{\partial z} + G(t) + \left( \frac{1}{r} \frac{\partial}{\partial r} (r S^{rz}) + \varepsilon^2 \frac{\partial}{\partial z} (S^{zz}) \right), \tag{3.13}$$

$$\begin{aligned} \psi e p_r \left( \frac{\partial T}{\partial t} + \varepsilon \left( \sigma u \frac{\partial T}{\partial r} + v \frac{\partial T}{\partial z} \right) \right) &= B_r \left( \sigma \varepsilon^2 S^{rr} \frac{\partial u}{\partial r} + S^{rz} \frac{\partial v}{\partial r} + \sigma \varepsilon^2 S^{zr} \frac{\partial u}{\partial z} + \varepsilon^2 S^{zz} \frac{\partial v}{\partial z} \right) \\ &+ \left( \frac{\partial^2 T}{\partial r^2} + \frac{1}{r} \frac{\partial T}{\partial r} + \varepsilon^2 \frac{\partial^2 T}{\partial z^2} \right). \end{aligned} \tag{3.14}$$

The components of  $S^{ij}$  extra stress are given:

$$S^{rz} = (M + (1 - M)S) \left( \frac{\partial v}{\partial r} + \sigma \frac{\partial u}{\partial z} \right),$$

$$S^{rr} = (M + (1 - M)S) \left( \varepsilon \sigma \frac{\partial u}{\partial r} \right),$$

$$S^{zz} = (M + (1 - M)S) \left( \varepsilon \frac{\partial v}{\partial z} \right),$$

$$S = \left( 1 + \left\{ We^2 \left[ \left| 2 \left( \sigma \varepsilon \left( \left( \frac{\partial u}{\partial r} \right)^2 + \left( \frac{u}{r} \right)^2 \right) + \varepsilon \left( \frac{\partial v}{\partial z} \right)^2 \right) + \left( \sigma \frac{\partial u}{\partial z} + \frac{\partial v}{\partial r} \right)^2 \right| \right] \right\}^{\frac{n-1}{2}} \right)^{-1}. \quad (3.15)$$

The parameters should be used in non-dimensional form in order to maintain modeling:

$$u = \frac{u^* l_0}{\sigma^* U_0}, \quad y = \frac{v^*}{U_0}, \quad r = \frac{r^*}{a}, \quad z = \frac{z^*}{l_0}, \quad t = \frac{t^* U_0}{a}, \quad R = \frac{R^*}{a},$$

$$p = \frac{p^* a^2}{l_0 \mu_0 U_0}, \quad l_0 = \frac{l_0^*}{R_0}, \quad S^{rr} = \frac{l_0}{U_0 \mu_0} S^{*rr}, \quad S^{zz} = \frac{l_0}{U_0 \mu_0} S^{*zz},$$

$$S^{rz} = \frac{a}{U_0 \mu_0} S^{*rz}, \quad We = \frac{G U_0}{a}, \quad Re = \frac{\rho U_0 a}{\mu_0}, \quad M = \frac{\mu_8}{\mu_0},$$

$$\beta_I = \frac{\beta_I^*}{l_0}, \quad Pr = \frac{C_p \mu_0}{k}, \quad B_r = \frac{\mu_0 U_0^2}{k(T_l)}, \quad T^* = \frac{T}{T_1}, \quad (3.16)$$

where  $U_0$  is the average velocity of unstable flow with a dimensionless number. Also,  $Re$ ,  $We$ ,  $Pr$ ,  $\frac{\partial p}{\partial z}$  are the symbols for Reynolds number, Weissenberg number, Prandtl number and the pulsatile pressure gradient for the human body. Therefore,

$$-\frac{\partial p}{\partial z} = D_1(1 + e \cos(\alpha_2 t + \phi)). \quad (3.17)$$

The periodic oscillations of the body for  $t > 0$  can be characterized by

$$G(t) = D_2 \cos(\alpha_2 t + \phi), \quad (3.18)$$

where  $\phi$  describes the difference in phases

$$\alpha_1 = \frac{a \omega_p}{U_0}, \quad D_1 = \frac{A_0 a^2}{\mu_0 U_0}, \quad D_2 = \rho A_g \frac{a^2}{\mu_0 U_0}, \quad G(t) = \frac{\rho a^2 G^*(t^*)}{U_0 \mu_0}, \quad e = \frac{A_1}{A_0}, \quad \alpha_2 = \frac{a \omega_0}{U_0}. \quad (3.19)$$

## 4. Methodology

No one may consider the time-dependent geometry of stenosis by tapered artery because of the preceding discussion through literature review. As a consequence, the time-dependent geometry of stenosis in tapered arteries has been taken into account. The casson fluid model is used to treat our blood. Graphs are used to calculate velocity, wall shear stress, and flow rate. The COMSOL(4.1) Multi-physics; a simulation software has been used in this study. MATLAB is used to measure the numerical values, which are then compared to theoretical and experimental data. In terms of boundary conditions, we embraced an oscillatory physiological velocity profile on the input boundary  $z = 0$  in order to simulate heart beats (1s periodic function).

$$u = 0, \quad v = F(t) \left( 1 - \left( \frac{r}{R} \right)^2 \right).$$

Here,

$$f(t) = \frac{a_0}{2} + \sum_{k=1}^7 (a_k \cos(2\pi kt) + b_k \sin(2\pi kt)). \quad (4.1)$$

Fourier decomposition of spatial average velocity:

$$V_m = \frac{1}{T} \int_0^T \bar{v}(t) \exp(-jm\omega t) dt.$$

The spatial average velocity is then

$$\bar{v}(t) = v_0 + \sum_{m=1}^{\infty} |V_m| \cos(m\omega t - \phi_m). \tag{4.2}$$

## 5. The Problem's Resolution

### 5.1 Perturbation Solution

Any issue concerning the interaction of fluid mechanics and vessel wall mechanics, Instead of having its unique form as an input,  $\psi(z, t)$  may normally be extracted as part of the solution. Since  $\psi(z, t)$  is clearly established in this case, our focus will be solely on the haemodynamic factors. Non-dimensional field equations can be used to propagate blood flow [23] in elastic arteries [42]

$$\begin{aligned} 2\frac{\partial u}{\partial t} + 2\omega \left[ f' + \frac{\partial u}{\partial z} \right] + [\lambda_\theta + f(z) + u] \frac{\partial \omega}{\partial z} &= 0, \\ \frac{\partial u}{\partial t} + \omega \frac{\partial \omega}{\partial z} + \frac{\partial p}{\partial z} - v \left[ \frac{\partial^2 \omega}{\partial z^2} - \frac{8\omega}{(\lambda_\theta + f(z) + u)^2} \right] &= 0, \\ p = \frac{m}{\lambda_z(\lambda_\theta + f(z) + u)} \frac{\partial^2 u}{\partial t^2} + \frac{1}{\lambda_z(\lambda_\theta + f(z) + u)} \frac{\partial \pi}{\partial \lambda_2} - \frac{1}{(\lambda_\theta + f(z) + u)} \frac{\partial}{\partial z} \left( \frac{f' + \frac{\partial u}{\partial z}}{\Lambda} \right) \frac{\partial \pi}{\partial \lambda_1} \\ + \frac{4v(f' + \partial(u)/\partial(z)\omega)}{\lambda_\theta + f(z) + u}, \end{aligned} \tag{5.1}$$

where  $u$  indicates the radial motion,  $\omega$  specifies the axial velocity on average,  $p$  presents the fluid pressure on average,  $v$  means the fluid's viscosity and  $f(z)$  is a function that defines the variance of a radius in the axial direction. (In this situation, Dilatation (aneurismal [49]) geometry is defined by  $f$ . The in-compressible state (mass conservation) of the fluid is expressed by the first equation of (5.1), which is a conservative fluid momentum equation. By using Newton's second law, the third equation of (5.1) is obtained. Where the density of the material's strain energy feature is  $\pi$ .  $m$  is the relative mass of the wall. In both circumferential and axial directions, the initial stretch ratios were determined that are  $\lambda_\theta, \lambda_z$ , successively. In both circumferential and axial directions, the current stretch ratios are  $\lambda_1, \lambda_2$  and  $\Lambda = [1 + f' + \frac{\partial u}{\partial z}]^{\frac{1}{2}}$ .

In comparison with equation (5.1) research, the reductive impatience approach is used to study the dispersive wave propagation in a fluid-solid structure system. The reductive perturbation method was developed for long-wave approximation. The following expanded coordinates are added

$$\xi = \epsilon^{1/2}(z - ct), \quad \tau = \epsilon^{3/2}z, \tag{5.2}$$

where  $\epsilon$  is a small parameter that calculates the dispersion weakness and  $c$  is the phase velocity in the long-wave limit. Then  $z = \epsilon^{-3/2}\tau$  and  $f(\epsilon^{-\frac{3}{2}}\tau) = x(\xi, \tau)$ . Considering the effect of dilatation,

it is presumed that  $f$  to be of the order of  $5/2$  i.e.

$$x(\xi, \tau) = \epsilon h(\tau). \quad (5.3)$$

Furthermore, considering the effect of viscosity, It is presumed that the order of viscosity will be  $O(3/2)$ , i.e.

$$v = \epsilon^{3/2} \bar{v}. \quad (5.4)$$

Establishing the subsequent perturbation development of the variables  $u$ ,  $\omega$  and  $p$  in term of  $\epsilon$

$$\begin{aligned} u &= \epsilon u_1 + \epsilon^2 u_2 + \dots \\ \omega &= \epsilon \omega_1 + \epsilon^2 \omega_2 + \dots \\ p &= p_0 + \epsilon p_1 + \epsilon^2 p_2 + \dots \end{aligned} \quad (5.5)$$

Substituting equations (5.2)-(5.5) into equation (5.1), the following differential sets are obtained:

$O(\epsilon)$  **Equation**

$$\begin{aligned} -2c \frac{\partial u_1}{\partial \xi} + \lambda_\theta \frac{\partial \omega_1}{\partial \xi} &= 0, \\ -c \frac{\partial \omega_1}{\partial \xi} + \frac{\partial p_1}{\partial \xi} &= 0, \\ p_1 &= \gamma_1(u_1 + h(r)). \end{aligned} \quad (5.6)$$

$O(\epsilon^2)$  **Equation**

$$\begin{aligned} -2c \frac{\partial u_2}{\partial \xi} + 2\omega_1 \frac{\partial u_1}{\partial \xi} + \lambda_\theta \frac{\partial \omega_2}{\partial \xi} + [u_1 + h] \frac{\partial u_1}{\partial \xi} + \lambda_\theta \frac{\partial \omega_1}{\partial \tau} &= 0, \\ -c \frac{\partial \omega_2}{\partial \xi} + \omega_1 \frac{\partial \omega_1}{\partial \xi} + \frac{\partial p_2}{\partial \xi} + \frac{\partial p_1}{\partial \tau} + \frac{8\bar{v}\omega_1}{\lambda_\theta^2} &= 0, \\ p_2 &= \left( \frac{mc^2}{\lambda_\theta \lambda_z} - \gamma_0 \right) \frac{\partial^2 u_1}{\partial \xi^2} + \gamma_1 u_2 + \gamma_2 u_1^2 + 2\gamma_2 h(\tau) u_1 + \gamma_2 h^2(\tau), \end{aligned} \quad (5.7)$$

where

$$\begin{aligned} \beta_0 &= \frac{1}{\lambda_\theta \lambda_z} \frac{\partial \Pi}{\partial \lambda_\theta}, \\ \beta_1 &= \frac{1}{\lambda_\theta \lambda_z} \frac{\partial \Pi}{\partial \lambda_\theta^2}, \quad \beta_2 = \frac{1}{2\lambda_\theta \lambda_z} \frac{\partial^3 \Pi}{\partial \lambda_\theta^3}, \\ \gamma_1 &= \beta_1 - \frac{\beta_0}{\lambda_\theta}, \quad \gamma_2 = \beta_2 - \frac{\beta_1}{\lambda_\theta}. \end{aligned} \quad (5.8)$$

In view of the process in infinity, the following equation can be written as the solution of the equation (5.5)

$$u_1 = U(\xi, \tau), \quad \omega_1 = \frac{2c}{\lambda_0} U, \quad p_1 = \frac{2c^2}{\lambda_0} U + \gamma_1 h(\tau), \quad \gamma_1 = 2 \frac{c^2}{\lambda_\theta}. \quad (5.9)$$

If  $U(\xi, \tau)$  is an unidentified function, the governing equation is achieved as follows. Here, we introduced equation (5.8) in equation (5.6), and the nonlinear equation of evolution is achieved

through some mathematical transformations

$$\frac{\partial U}{\partial \tau} = \mu_1 U \frac{\partial U}{\partial \xi} + \mu_2 \frac{\partial^3 U}{\partial \xi^3} + \mu_3 U + \mu_4(\tau) = 0,$$

where

$$\mu_1 = \frac{5}{2\lambda_\theta} + \frac{\gamma_2}{\gamma_1},$$

$$\mu_2 = \frac{m}{4\lambda_z} - \frac{\gamma_0}{2\gamma_1}, \tag{5.10}$$

$$\mu_3 = 4\bar{v}v \frac{2}{\gamma_1 \lambda_\theta^5}, \tag{5.11}$$

$$\mu_4(\tau) = h(\tau) \left( \frac{1}{2\lambda_\theta} + \frac{\gamma_2}{\gamma_1} \right), \tag{5.12}$$

$$\mu(\tau) = \frac{1}{2} h'(\tau). \tag{5.13}$$

### 5.2 Expression for Wall Shear Stress and Resistance Impedance

The profiles of velocity are estimated so far then the dimensionless relationships for the volumetric flow rate are calculated, the impedance of wall shear stress [46] and resistance is measured as follows [19].

$$Q_i^k = \int_0^R v r dr$$

$$\Lambda_i^k = \frac{(|L(\frac{\partial p}{\partial z})_i^k|)}{Q_i^K}$$

$$\tau_s = \left\{ M + (1 - M) \left( 1 + \left( We^2 \left| \frac{\partial v}{\partial r} \right|^2 \right)^{\frac{n-1}{2}} \right)^{-1} \right\} \frac{\partial v}{\partial r}. \tag{5.14}$$

A coordinate conversion can be applied to the governing artery as  $k = r/\psi$  to describe the motionless elastic artery, initial and boundary equations.

As a result, the mesh grids can therefore be created on the artery’s applied cross-section region. The following equations will result in the application of the described coordinate conversion.

$$\frac{\partial v}{\partial t} = \frac{1}{Re} \left( D_1(1 + e \cos(\alpha_1 t)) + \frac{1}{k\psi^2} \frac{\partial}{\partial k} \left[ k \left\{ M + (1 - M) \left( 1 + \left( \left( \frac{We}{R} \right)^2 \left| \frac{\partial v}{\partial K} \right|^2 \right)^{\frac{n-1}{2}} \right)^{-1} \right\} \frac{\partial v}{\partial K} \right] \right), \tag{5.15}$$

$$\frac{\partial T}{\partial t} = \frac{Br}{\psi e Pr R^2} \left\{ M + (1 - M) \left( 1 + \left( \left( \frac{We}{\psi} \right)^2 \left| \frac{\partial v}{\partial K} \right|^2 \right)^{\frac{n-1}{2}} \right)^{-1} \right\} \left( \frac{\partial v}{\partial K} \right)^2 + \frac{1}{\psi^2} \left\{ \frac{\partial^2 T}{\partial K^2} + \frac{1}{K} \frac{\partial T}{\partial k} \right\}. \tag{5.16}$$

The dimensionless relationships are like in the case of initial circumstances,

$$v(r, 0) = 2U_0(1 - k^2), \quad T(k, 0) = 0. \tag{5.17}$$

and for the boundary conditions:

$$\begin{aligned} \frac{\partial v(k,t)}{\partial k} &= 0, \quad \frac{\partial T}{\partial K} = 0, \quad K = 0, \\ v(k,t) &= 0, \quad T(k,t) = 1, \quad k = 1 \end{aligned} \quad (5.18)$$

## 6. Result Analysis

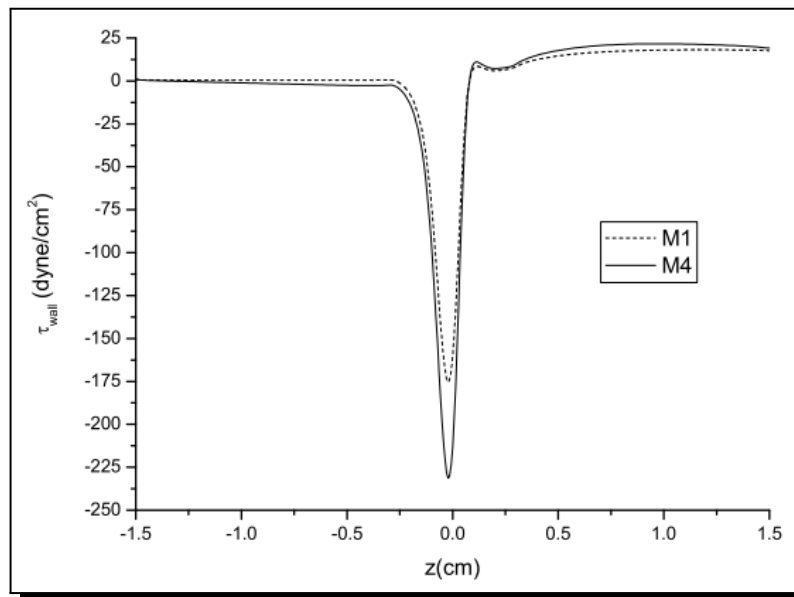


**Figure 9.** Wall shear stress distributions along the vessel wall at  $t/T = 0.5$

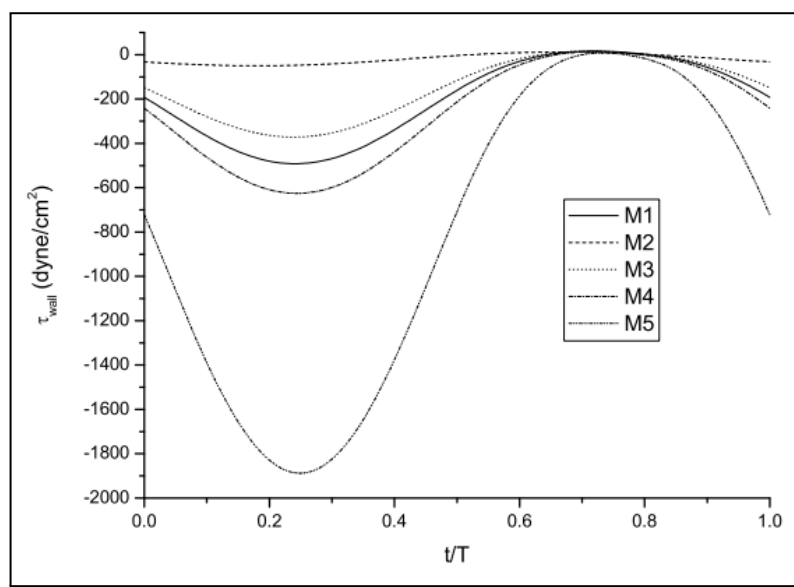


**Figure 10.** The wall shear stress distributions at the stenosis's throat

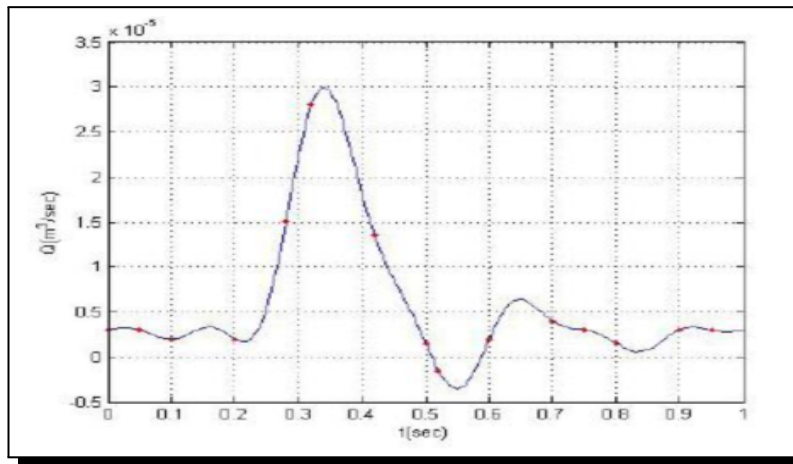


**Figure 11.** The volumetric flow rate of pulsatile

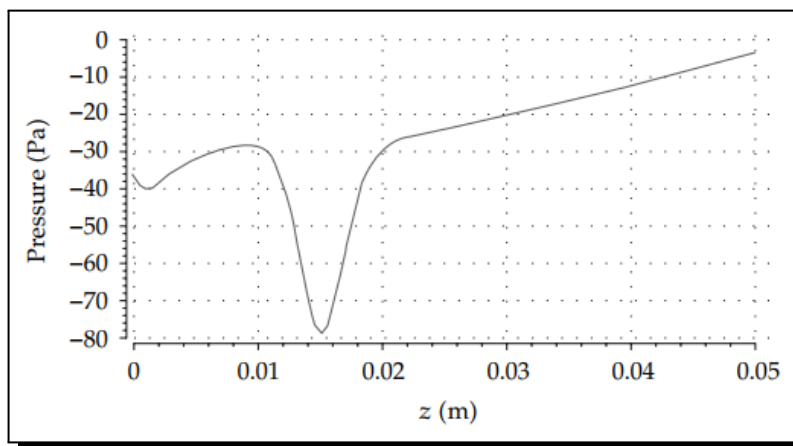


**Figure 12.** At peak systole, pressure along a longitudinal line was linked to stenosed vessels with severity levels of 30%

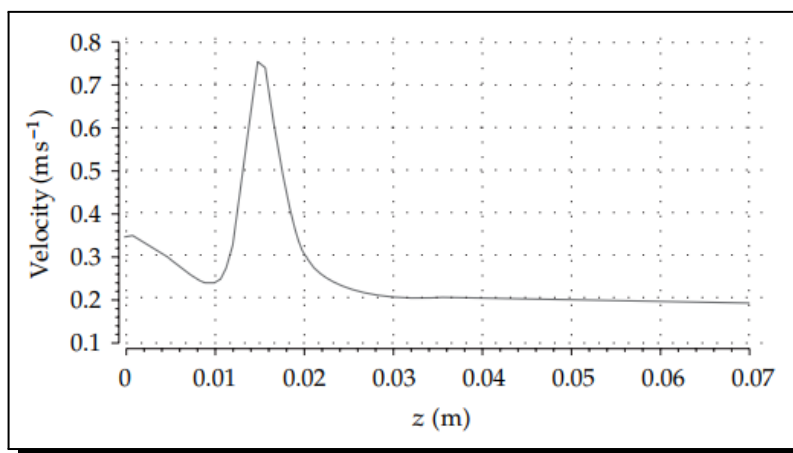


**Figure 13.** At peak systole, pressure along the longitudinal line was compared to stenosed vessels with severities of 50%

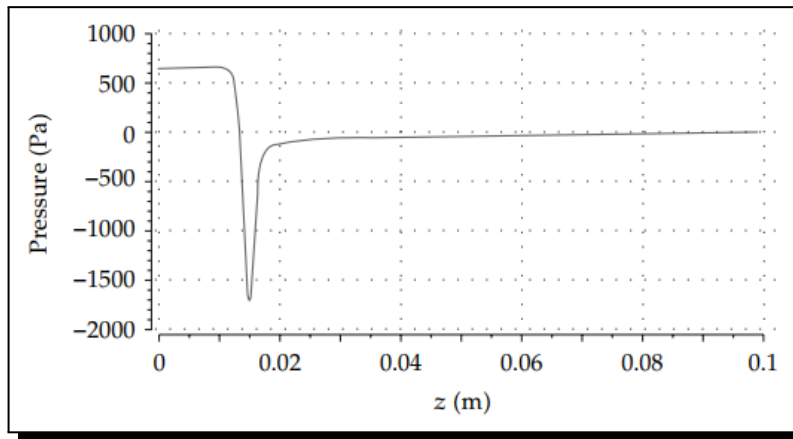


**Figure 14.** At peak systole, pressure along a longitudinal line was compared to stenosed vessels with severities of 70%

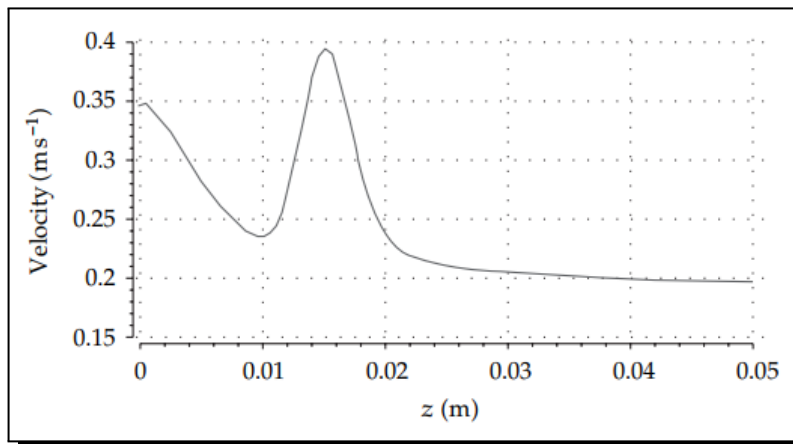


**Figure 15.** Blood flow velocity alongside a longitudinal line at peak systole in vessels with stenosis severity of 30%

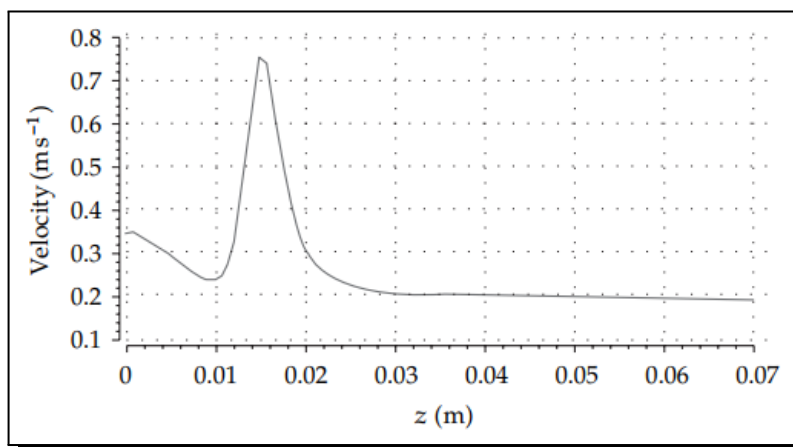


**Figure 16.** Blood flow speed along a longitudinal line at peak systole in vessels with stenosis severity of 50%

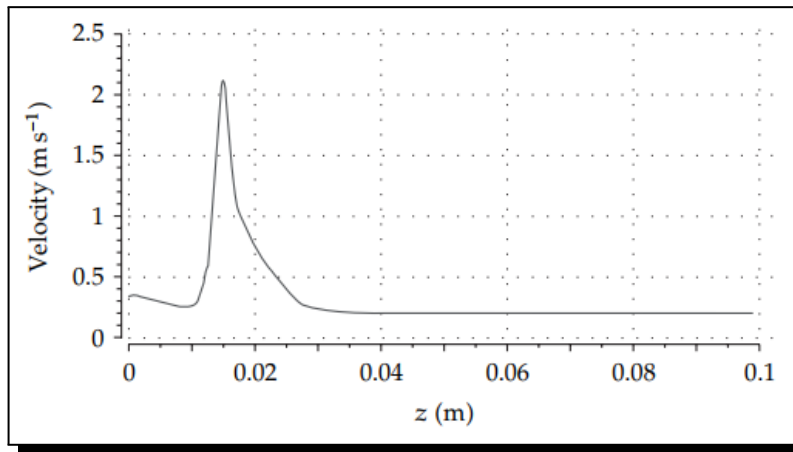


**Figure 17.** Blood flow velocity along a longitudinal line at peak systole in stenosed vessels with severities of 70%

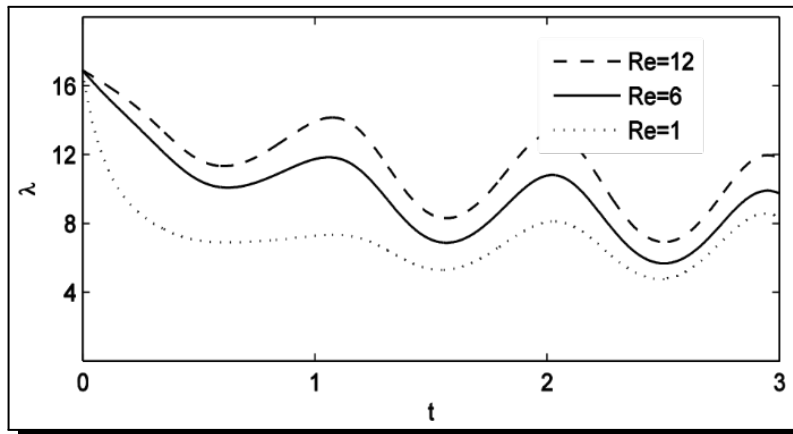


**Figure 18.** Resistance impedance varies for different Reynolds numbers

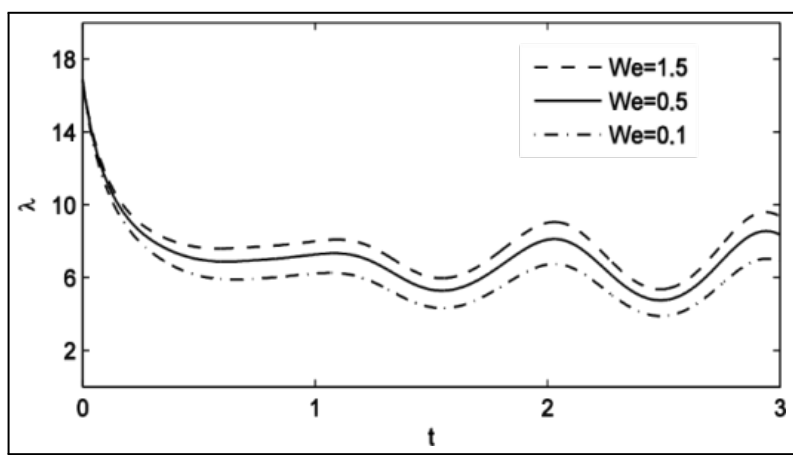


**Figure 19.** Resistance impedance variation for various wissenberg numbers

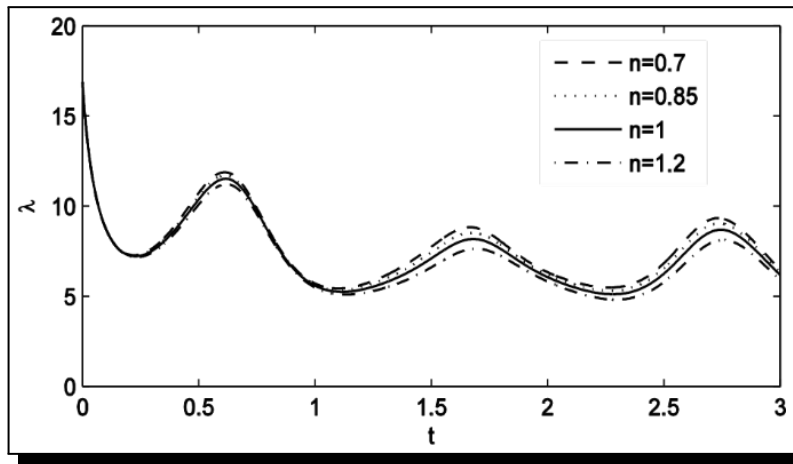


Figure 20. Resistance impedance varies depending on the aneurysm’s form

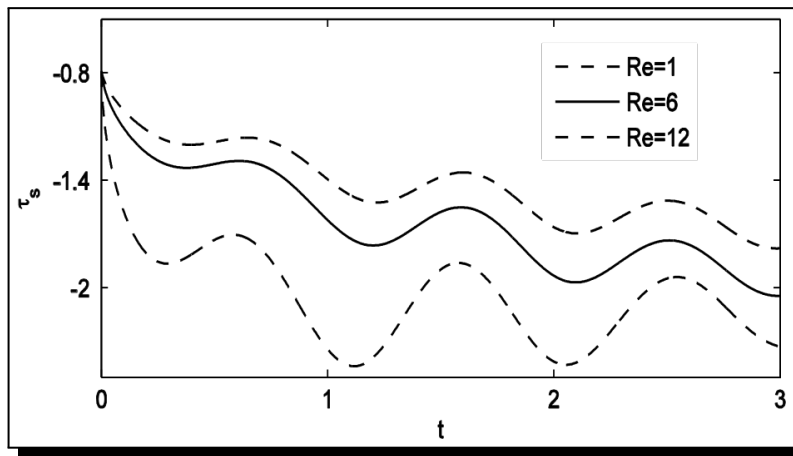


Figure 21. Wall shear stress variation for various Reynolds numbers

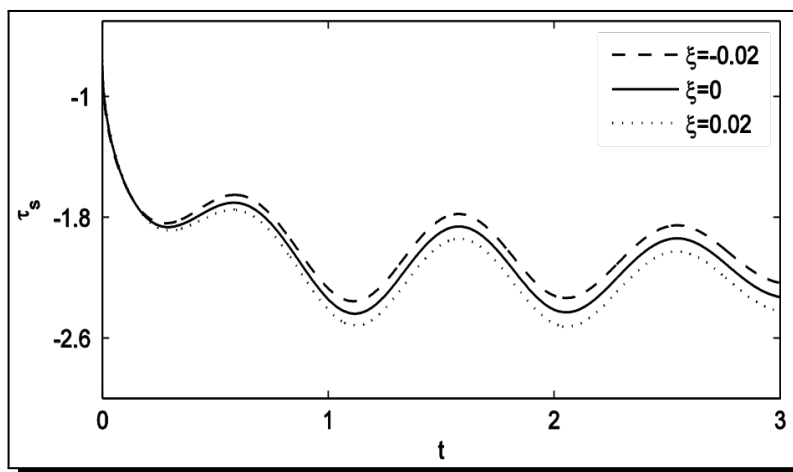


Figure 22. Wall shear stress variation for different tapered angles

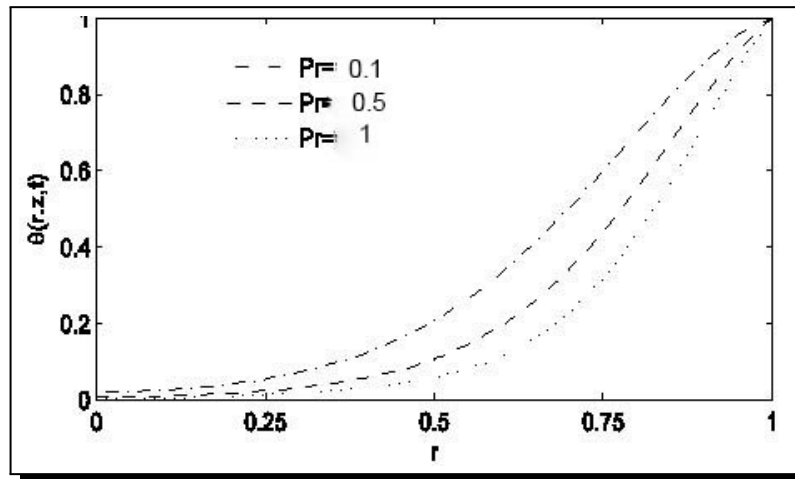


Figure 23. For different prandtl numbers, the wall shear stress varies

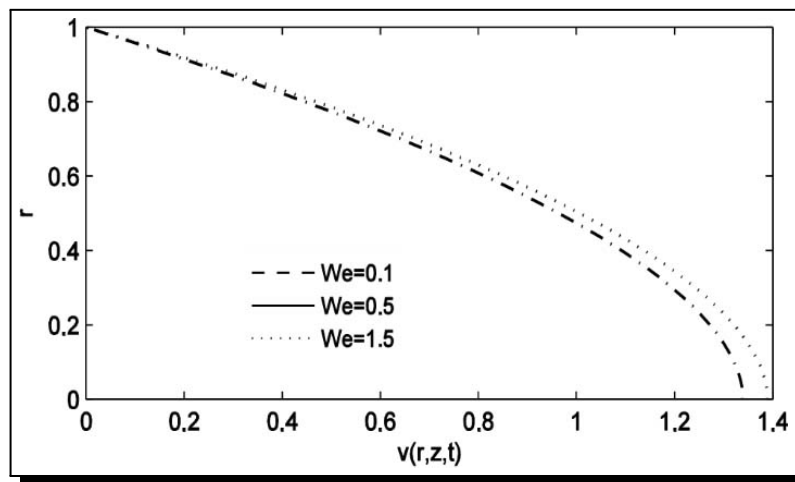


Figure 24. For different weissenberg numbers, the velocity side view varies

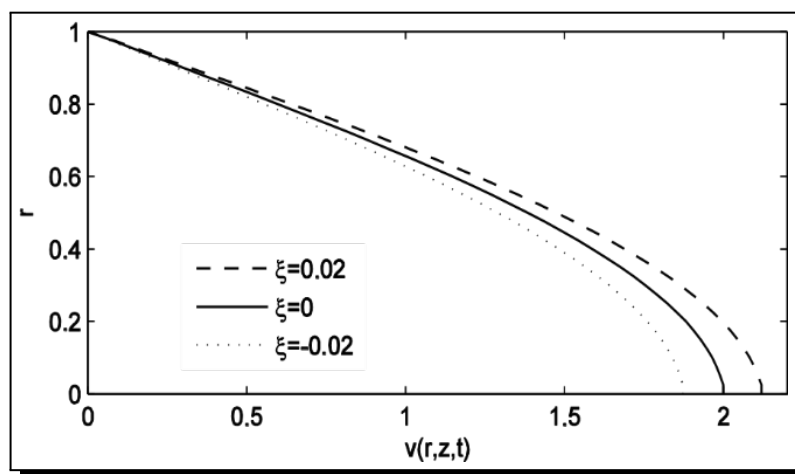


Figure 25. For various tapered angles, the velocity side view varies

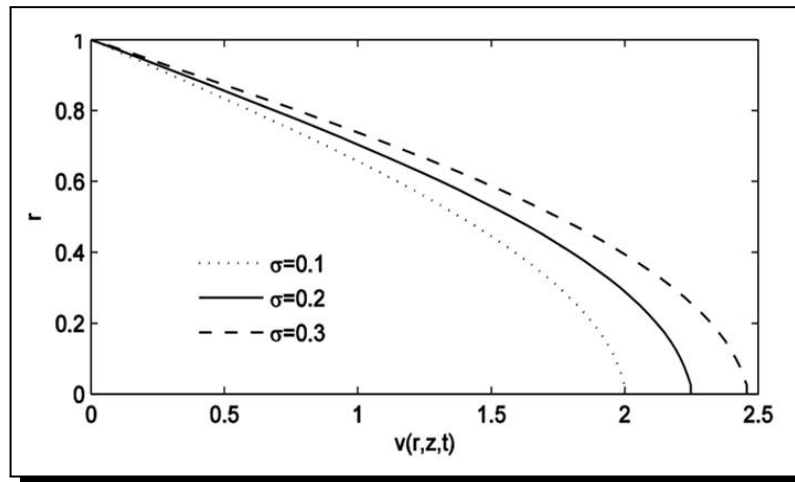


Figure 26. Variation of the velocity outline for various aneurysm radial values

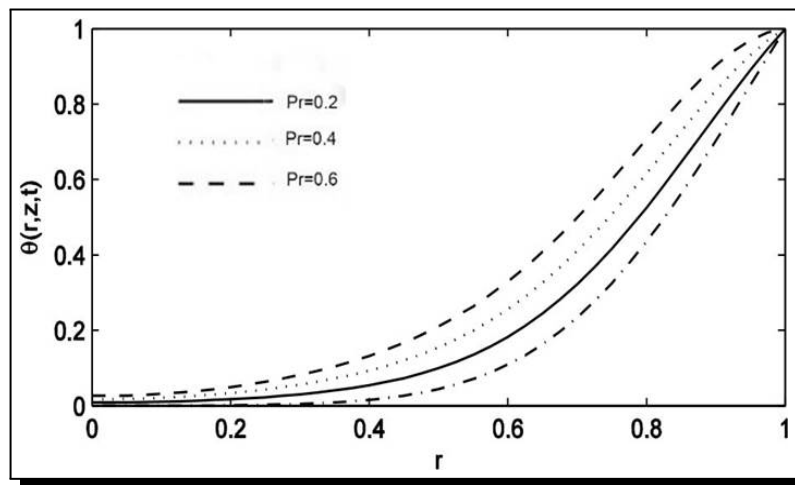


Figure 27. For various prandtl numbers, a variation of dimensionless temperature side view is shown

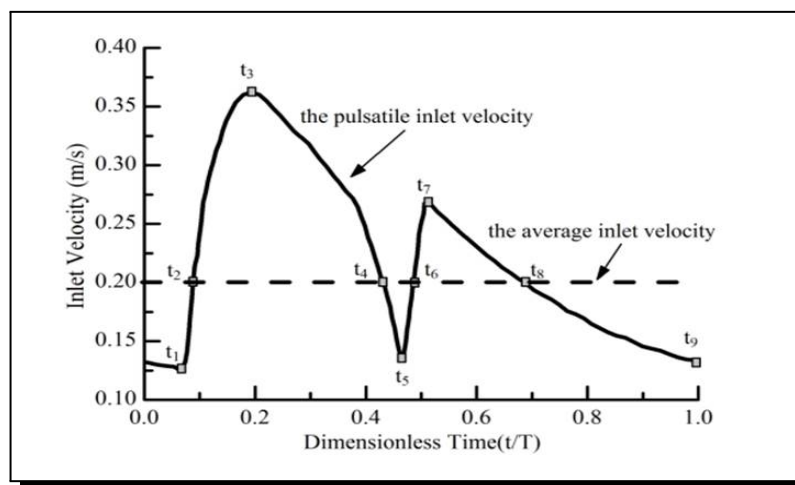


Figure 28. In the inlet for blood flow, the average velocity and pulsatile velocity waveforms are shown

The cardiac cycle length,  $T = 0.735$  s, is used to scale the dimensional less time  $t/T$ .

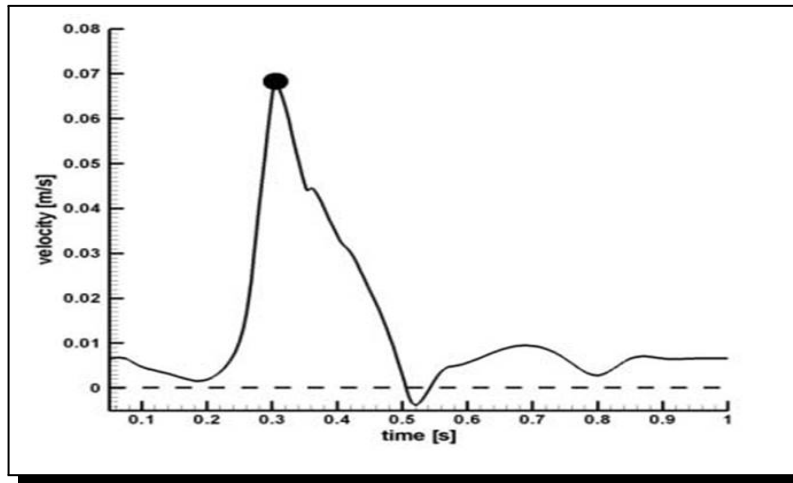


Figure 29. Velocity group

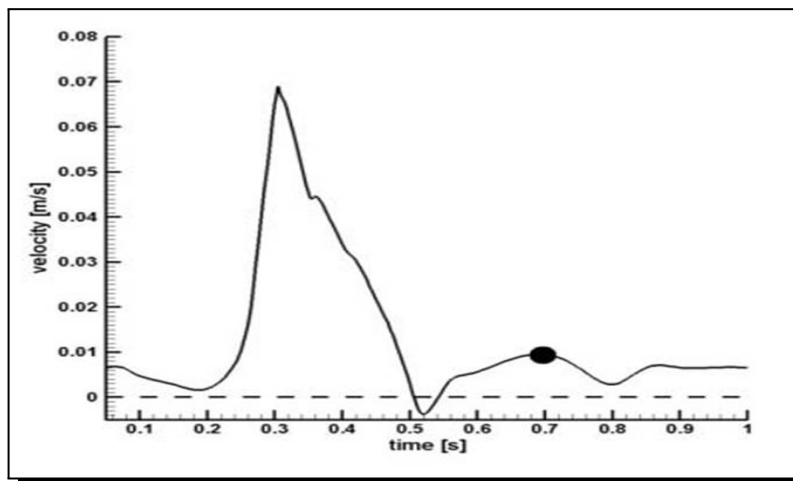


Figure 30. Velocity group

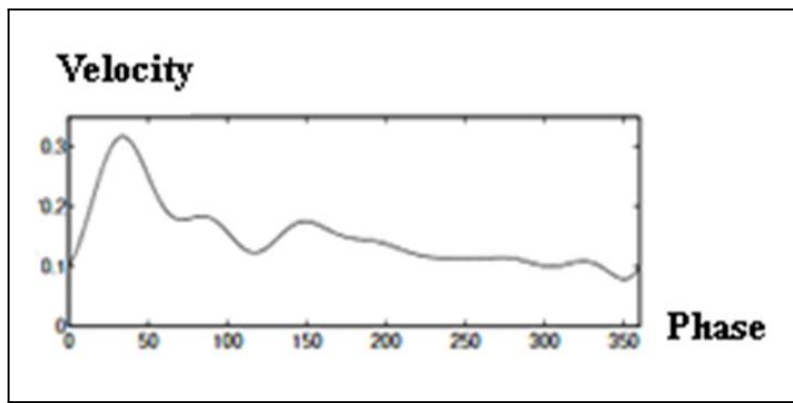


Figure 31. Mean velocities in space from the common femoral artery (top)

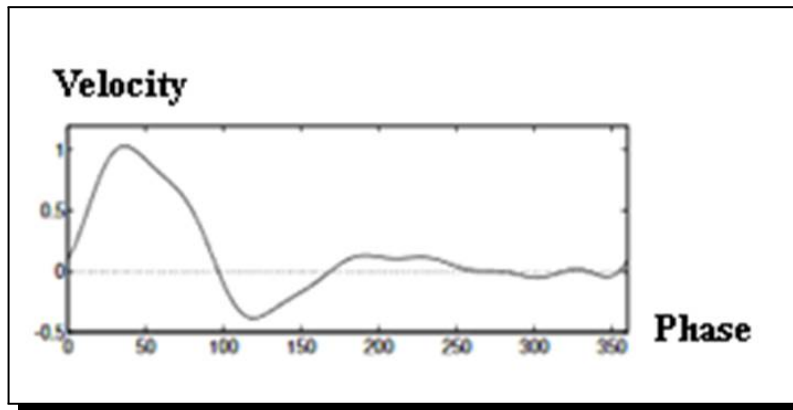


Figure 32. The carotid arteries' spatial mean velocities (bottom)

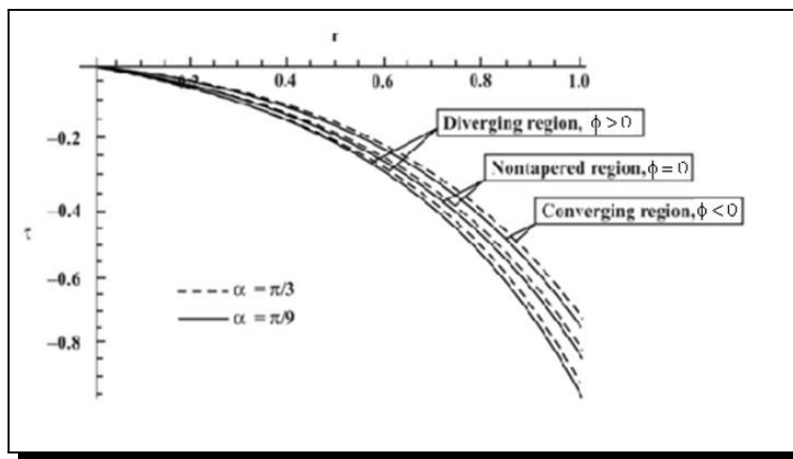


Figure 33. For various values of tapering angle, the effect of artery inclination on shearing stress

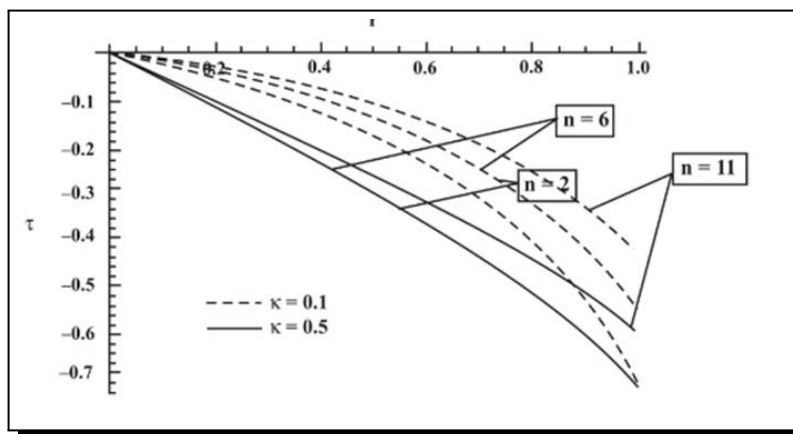


Figure 34. For various values of the shape parameter ( $n$ ) and permeability, the effect of permeability on the shearing stress was investigated ( $k$ )

## 7. Discussion

In order to estimate the effect of tapering on the wall shear stress, we give the results for the allocations of the wall shear stress through models M1 and M4 at  $t/T = 0.5$  (Figure 9). Figure 9 shows that the variation of the shear stress of wall is almost the same except at the throat of the stenosis. Due to the tapering, the maximal negative value is bigger near the throat of the stenosis. We also compare the results at other times finding that the situation is the same as that at  $t/T = 0.5$ . Figure 10 illustrates the results for the distribution of the wall shear stress at the throat of the stenosis; it is well known that at this location the values of the wall shear stress are the highest. With the value of  $h$  increasing, the oscillation amplitude of the wall shear stress increases.

Wall shear stress is a key factor for the study of blood flow. Correct estimation of wall shear stress distribution is relevant in the knowledge of the effects of blood flow on endothelial cells. Numerical studies have been conducted through various types of stenotic and tapered vessels with laminar flow, rigid walls, and Newtonian fluid. The study found that the height of stenosis had a significant effect on the wall shear stress in the throat and downstream of the throat. Owing to the tapering, the oscillation amplitude of the shear stress of the wall is higher than that of the untapped artery.

We plotted graphs of the stress on the wall glass and considered the effect of different types of pressure on the light aneurysm curved arteries. Aneurysm, velocity, temperature and various emerging flow parameters to prevent blood flow obstruction. The emerging flow parameters are aneurysm shape, Prandtl numbers, Weissenberg number, Reynolds number and shear-thinning fluid parameter. It is possible to understand the impact of contraction by holding the limit constant to understand the limit of the flow.

Figure 18 efforts to show that the upgraded Reynolds numbers (1, 6, and 12) can provide substantial impedance increases in various situations. Similarly, it is likely to feel that the volumetric flow rate has the opposite effect on blood flow obstruction. The Weissenberg numbers at various periods (0.1, 0.5, and 1.5, respectively) are shown in Figure 19.

Figure 20 shows the flow obstruction of aneurysms of various shapes at various timings. According to these results, the expansion of the shape causes the protection of blood flow from decline, or in short, as the  $n$  parameter increases, the reaction force of the blood flow decreases. As the relevant Reynolds numbers (1, 6, and 12) expand in Figure 21, the pressure divider's shear pressure can be increased. The contour's mathematics focuses on the estimation of the separation line shear pressure of the tightened and un-tightened veins in Figure 22. At the point where this point gradually expands, the sheer pressure of the dividing line is relieved. Also, it is noteworthy that the tendency of the non-tapered blood vessel is situated in the curve that includes the open and close-ended arteries.

Figure 23 indicates that Wall shear pressure increases as the number of Prandtl aneurysms (for 0.1, 0.5, and 1) increases. The type of arterial axial velocity with various tapered angles

of the aneurysm is presented in Figure 13. The axial velocity inside the artery is gradually adjusted with growing angles. Likewise, the result of an un-tightened catheter is to merge and bend the twisted blood vessel. These findings are in close agreement with the observation that an aneurysm greatly affects blood flow and re-circulation.

Figure 26 shows the hub velocity distribution inside the flexible artery compared to three unique aneurysm values ( $\sigma=0.1$ ,  $\sigma=0.2$ , and  $\sigma=0.3$ ) at two essential focal points  $z = 0.7$  and  $z = 2.1$ . Moreover, the pivoting speed increases as the aneurysm expands.

In simulations, two separate flow waveforms of the inlet velocity are used, as shown in Figure 16. Three different inlet velocities at time point's  $t_1$ ,  $t_2$ , and  $t_3$  (as shown in Figure 16) reflect the minimum inlet velocities in the pulsatile inlet state, they are chosen to study the WSS distributions because of their average and maximum velocity. In the same inlet conditions, WSS for non-Newtonian blood models are all higher than those for Newtonian blood models. After all, at the same inlet velocity of 0.2 m/s (steady and pulsatile ( $t_1$ )), the WSS distributions for the same blood model (Newtonian or non-Newtonian) are entirely different. Furthermore, regardless of blood models, as inlet velocity increases, the WSS distributions increase. The pulsation of inlet conditions and blood models tend to have a significant effect on WSS distributions.

We used pulsatile flow of a power law fluid, and we modeled and analyzed it in the cardiovascular system. The form is used to investigate vital flow in stenotic arteries with varying degrees of stenosis 30%, 50%, and 70%. The minimum and maximum time stage for a 30% area severity are  $\Delta t_{\min} = 0.005$  s, and  $\Delta t_{\max} = 0.01$  s, respectively. The time stage are  $\Delta t_{\min} = 0.001$  s and  $\Delta t_{\max} = 0.005$  s for 50% and 70% area severity. As the occlusion approaches, there is a rapid drop in pressure. Greater pressure decreases around the stenosis as the percentage area severity increases (Figures 12, 13, and 14). In the stenosis region, it also results in faster speeds (Figures 15, 16, and 17). The findings obviously demonstrate the relationship between pressure and velocity. It demonstrates that pressure falls rapidly at the stenosis site, resulting in a jet flow at the stenosis's throat. If there is a negative pressure gradient at the stenosis site, the flow accelerates. When there is an adverse pressure slope, the flow slows. This additional pressure leap aids in propelling the flow through the narrowing channel. Comparing the outcomes of three stenotic tubes with region severity of 30 percent, 50 percent, and 70 percent. We discovered that stenosis an area with a greater percentage severity produces higher extra pressure jumps. The plot groups for the blood velocity profile based on the width of the artery at time  $t = 0.302$  s,  $t = 0.52$  s,  $t = 0.3$  s and  $t = 0.7$  s are shown in Figures 29 and 30.

By the inspection of the Figure 33, it can be noticed that the converging region ( $\phi < 0$ ), in comparison to the diverging area, the stress will be higher ( $\phi > 0$ ) and non tapered region ( $\phi = 0$ ) that is, as the tapering angle increases, the wall shear stress increases ( $\phi$ ). Figure 34 depicts that the variation of wall stress  $\tau$ , with shape parameter  $n$  and permeability. It is evident that the pressure on the walls is lessening with increases of permeability parameter.

Blood flows from the left side into this horizontal flow channel and reaches the parabolic velocity profile resulted in a pressure gradient at the inlet and the outlet. The fluid velocity is much varied in the aneurysm region. The bifurcation of the vessels [8] creates a velocity profile skewed towards the inside walls of the vessels [8]. If blood velocity in the aneurysmal region is sufficiently low, small blood clots can site at the outside wall and travel with the bloodstream with the risk of causing a stroke.

## 8. Conclusion

From the results, it can be inferred that compared and patented aneurysms, aneurysms that are completely blocked during development are moderately necked and have a longer standard travel time. In the area of the aneurysm, the pressure of the dividing line is shallow. As the size of the aneurysm increases, the sheer pressure of the dispenser decreases. Increase the flow rate by expanding the size of the aneurysm. A basic understanding of atherosclerosis, ICAs, improved clinical arrangements as treatment methods, medical consultants, and prudent strategies gradually adopted can reduce disease-related depression and mortality. The scale of the stenosis in stenosed vessels has an effect on blood flow, according to our findings. The blood flow rate changes drastically when the cross-sectional value is changed significantly. It is also apparent that as the permeability parameter is increased, the wall stress decreases.

### Competing Interests

The authors declare that they have no competing interests.

### Authors' Contributions

All the authors contributed significantly in writing this article. The authors read and approved the final manuscript.

## References

- [1] H. Abe, K. Hayashi and M. Sato (eds.), *Data Book on the Mechanical Properties of Living Cells, Tissues, and Organs*, Springer, Tokyo (1996), <https://www.springer.com/gp/book/9784431701750>.
- [2] S. A. Ahmed, An experimental investigation of pulsatile flow through a smooth, *Experimental Thermal and Fluid Science* **17** (1998), 309 – 318, DOI: 10.1016/S0894-1777(98)00009-0.
- [3] L. Ai and K. Vafai, An investigation of Stokes' second problem for non-Newtonian fluids, *Numerical Heat Transfer, Part A: Applications* **47**(10) (2005), 955 – 980, DOI: 10.1080/10407780590926390.
- [4] N. S. Akbar, S. Nadeem and C. Lee, Biomechanical analysis of Eyring Prandtl fluid model for blood flow in stenosed arteries, *International Journal of Nonlinear Sciences and Numerical Simulation* **14** (2013), 345 – 353, DOI: 10.1515/ijnsns-2012-0062.
- [5] H. I. Andersson, R. Halden and T. Glomsaker, Effects of surface irregularities on flow resistance in differently shaped arterial stenoses, *Journal of Biomechanics* **33**(10) (2000), 1257 – 1262, DOI: 10.1016/s0021-9290(00)00088-9.

- [6] İ. Bakırtaş and H. Demiray, Amplitude modulation of nonlinear waves in a fluid-filled tapered elastic tube, *Applied Mathematics and Computation* **154** (2004), 747 – 767, DOI: 10.1016/S0096-3003(03)00748-3.
- [7] İ. Bakırtaş and N. Antar, Evolution equations for nonlinear waves in a tapered elastic tube filled with a viscous fluid, *International Journal of Engineering Science* **41**(11) (2003), 1163 – 1176, DOI: 10.1016/S0020-7225(03)00005-3.
- [8] S. A. Berger and L.-D. Jou, Flows in stenotic vessels, *Annual Review of Fluid Mechanics* **32**(1) (2000), 347 – 382, DOI: 10.1146/annurev.fluid.32.1.347.
- [9] J. Bernsdorf and D. Wang, Non-Newtonian blood flow simulation incerebralaneyrums, *Computers & Mathematics with Applications* **58**(5) (2009), 1024 – 1029, DOI: 10.1016/j.camwa.2009.02.019.
- [10] C. Bertolotti and V. Deplano, Three-dimensional numerical simulations of flow through a stenosed coronary bypass, *Journal of Biomechanics* **33**(8) (2000), 1011 – 1022, DOI: 10.1016/s0021-9290(00)00012-9.
- [11] N. Bessonov, A. Sequeira, S. Simakov, Yu. Vassilevskii and V. Volpert, Methods of bloodflow modelling, *Mathematics Modelling of Natural Phenomena* **11**(1) (2016), 1 – 25, DOI: 10.1051/mmnp/201611101.
- [12] T. Canchi, S. D. Kumar, E. Y. Ng and S. Narayanan, A review of computational methods to predict the risk of rupture of abdominal aortic aneurysms, *BioMed Research International* **2015** (2015), Article ID 86162, DOI: 10.1155/2015/861627.
- [13] S. Chakravarthy, Sarifuddin and P. K. Mandal, Unsteady flow of a two-layer blood stream pasta tapered flexible artery under stenotic conditions, *Computational Methods in Applied Mathematics* **4** (2004), 391 – 409, DOI: 10.2478/cmam-2004-0022.
- [14] S. Chakravarty and A. K. R. Sannigrahi, A nonlinear mathematical model of blood flow in a constricted artery experiencing body acceleration, *Mathematical and Computer Modelling* **29** (1999), 9 – 25, <https://www.sciencedirect.com/science/article/pii/S0895717799000679/pdf?md5=268370df8a8d774b5907db66d874611f&pid=1-s2.0-S0895717799000679-main.pdf>.
- [15] A. J. Chorin and J. E. Marsden, *A Mathematical Introduction to Fluid Mechanics*, 3rd edition, Springer (1993), <https://bd.b-ok.africa/book/449688/baaaaf>.
- [16] V. Deplano and M. Siouffi, Experimental and numerical study of pulsatile flows through stenosis: wall shear stress analysis, *Journal of Biomechanics* **32**(10) (1999), 1081 – 1090, DOI: 10.1016/s0021-9290(99)00098-6.
- [17] O. Eytan, A. J. Jaffa and D. Elad, Peristaltic flow in a tapered channel: application to embryo transport within the uterine cavity, *Medical Engineering & Physics* **23**(7) (2001), 473 – 482, DOI: 10.1016/s1350-4533(01)00078-9.
- [18] E. A. Finol and C. H. Amon, Flow dynamics in anatomical models of abdominal aortic aneurysms: computational analysis of pulsatile flow, *Acta Científica Venezolana* **54** (2003), 43 – 49.
- [19] A. R. Haghighi and N. Pirhadi, A numerical study of heat transfer and flow characteristics of pulsatile blood flow in a tapered artery with a combination of stenosis and aneurysm, *International Journal of Heat and Technology* **37** (2019), 11 – 21, DOI: 10.18280/ijht.370102.
- [20] T. Hashimoto, H. Meng and W. L. Young, Intracranial aneurysms: Links among inflammation, hemodynamics and vascular remodeling, *Neurological Research* **28**(4) (2006), 372 – 380, DOI: 10.1179/016164106X14973.

- [21] T. Ishikawa, L. F. R. Guimaraes, S. Oshima and R. Yamane, Effect of non-Newtonian property of blood on flow through a stenosed tube, *Fluid Dynamics Research* **22**(5) (1998), 251 – 264, DOI: 10.1016/S0169-5983(97)00041-5.
- [22] M. Kothandapani and J. Prakash, Effect of radiation and magnetic field on peristaltic transport of nanofluids through a porous space in a tapered asymmetric channel, *Journal of Magnetism and Magnetic Materials* **378** (2015), 152 – 163, DOI: 10.1016/j.jmmm.2014.11.031.
- [23] M. Kothandapani and J. Prakash, Influence of heat source, thermal radiation and inclined magnetic field on peristaltic flow of a Hyperbolic tangent nanofluid in a tapered asymmetric channel, *IEEE Transactions on NanoBioscience* **14** (2015), 385 – 392, DOI: 10.1109/TNB.2014.2363673.
- [24] M. Kothandapani and J. Prakash, The peristaltic transport of Carreau Nanofluids under effect of a magnetic field in a tapered asymmetric channel: application of the cancer therapy, *Journal of Mechanics in Medicine and Biology* **15**(3) (2015), 1550030, DOI: 10.1142/S021951941550030X.
- [25] M. Kothandapani, J. Prakash and S. Srinivas, Peristaltic transport of a MHD Carreau fluid in a tapered asymmetric channel with permeable walls, *International Journal of Biomathematics* **8**(4) (2015), 1550054, DOI: 10.1142/S1793524515500540.
- [26] M. Kothandapani, J. Prakash and V. Pushparaj, Analysis of heat and mass transfer on MHD peristaltic flow through a tapered asymmetric channel, *Journal of Fluids* **2015** (2015), Article ID 561263, DOI: 10.1155/2015/561263.
- [27] D. Krex, H. K. Schackert and G. Schackert, Genesis of cerebral aneurysms – anupdate, *Acta Neurochirurgica* **143**(5) (2001), 429 – 449, DOI: 10.1007/s007010170072.
- [28] M. Kroon and G. A. Holzapfel, Modeling of saccular aneurysm growth in a human middle cerebral artery, *Journal of Biomechanical Engineering* **130**(5) (2008), 051012 (10 pages), DOI: 10.1115/1.2965597.
- [29] S. C. Ling and H. B. Atabek, A nonlinear analysis of pulsatile blood flow in arteries, *Journal of Fluid Mechanics* **55** (1972), 492 – 511.
- [30] G.-T. Liu, X.-J. Wang, B.-Q. Ai and L.-G. Liu, Numerical study of pulsating flow through a tapered artery with stenosis, *Chinese Journal of Physics* **42** (4-I), 401 – 409, <https://www.ps-taiwan.org/cjp/download.php?type=paper&vol=42&num=4-I&page=401>.
- [31] Q. Long, X. Y. Xu, K. V. Ramnarine and P. Hoskins, Numerical investigation of physiologically realistic pulsatile flow through arterial stenosis, *Journal of Biomechanics* **34**(10) (2001), 1229 – 1242, DOI: 10.1016/s0021-9290(01)00100-2.
- [32] J. J. V. McMurray and S. Stewart, The burden of heart failure, *European Heart Journal Supplements* **4**(6) (2002), 50 – 58, DOI: 10.1016/S1520-765X(02)90160-4.
- [33] Kh. S. Mekheimer and M. A. El Kot, Influence of magnetic field and hall currents on blood flow through a stenotic artery, *Applied Mathematics and Mechanics* **29** (2008), 1093 – 1104, DOI: 10.1007/s10483-008-0813-x.
- [34] Kh. S. Mekheimer and M. A. El Kot, Mathematical modelling of unsteady flow of a Sisko fluid through an anisotropically tapered elastic arteries with time-variant overlapping stenosis, *Applied Mathematical Modelling* **36** (2012), 5393 – 5407, DOI: 10.1016/j.apm.2011.12.051.
- [35] Kh. S. Mekheimer and M. A. El Kot, Suspension model for blood flow through arterial catheterization, *Chemical Engineering Communications* **197** (2010), 1195 – 1214, DOI: 10.1080/00986440903574883.

- [36] Kh. S. Mekheimer and M. A. El Kot, The micropolar fluid model for blood flow through a stenotic arteries, *International Journal of Pure and Applied Mathematics* **36** (2007), 393 – 405, <https://ijpam.eu/contents/2007-36-4/5/5.pdf>.
- [37] Kh. S. Mekheimer and M. A. El Kot, The micropolar fluid model for blood flow through a tapered artery with a stenosis, *Acta Mechanica Sinica* **24** (2008), 637 – 644, DOI: 10.1007/s10409-008-0185-7.
- [38] M. S. Moayeri and G. R. Zendehebudi, Effects of elastic property of the wall on flow characteristics through arterial stenoses, *Journal of Biomechanics* **36** (4) (2003), 525 – 535, DOI: 10.1016/S0021-9290(02)00421-9.
- [39] S. Mukhopadhyay and G. C. Layek, Analysis of blood flow through a modeled artery with an aneurysm, *Applied Mathematics and Computation* **217**(16) (2011), 6792 – 6801, DOI: 10.1016/j.amc.2010.10.011.
- [40] L. J. Myers and W. L. Capper, Exponential taper in arteries: an exact solution of its effect on blood flow velocity wave forms and impedance, *Medical Engineering & Physics* **26** (2004), 147 – 155, DOI: 10.1016/S1350-4533(03)00117-6.
- [41] M. Nakamura and T. Sawada, Numerical study on the unsteady flow of non-Newtonian fluid, *Journal of Biomechanical Engineering* **112**(1) (1990), 100 – 103, DOI: 10.1115/1.2891118.
- [42] E. V. Nikolova, On nonlinear waves in a blood-filled artery with an aneurysm, *AIP Conference Proceedings* **1978** (2018), 470050, DOI: 10.1063/1.5044120.
- [43] C. S. Peskin, Numerical analysis of blood flow in the heart, *Journal of Computational Physics* **25**(3) (1977), 220 – 252, DOI: 10.1016/0021-9991(77)90100-0.
- [44] G. Pontrelli, Pulsatile blood flow in a pipe, *Computers & Fluids* **27**(3) (1998), 367 – 380, DOI: 10.1016/S0045-7930(97)00041-8.
- [45] D. S. Sankar, A two-fluid model for pulsatile flow in catheterized blood vessels, *International Journal of Non-Linear Mechanics* **44** (2009), 337 – 351, DOI: 10.1016/j.ijnonlinmec.2008.12.008.
- [46] G. J. Sheard, Flow dynamics and wall shear stress variation in a fusiform aneurysm, *Journal of Engineering Mathematics* **64**(4) (2009), 379 – 390, DOI: 10.1007/s10665-008-9261-z.
- [47] M. Siouffi, V. Deplano and R. Pelissier, Experimental analysis of unsteady flows through a stenosis, *Journal of Biomechanics* **31**(1) (1998), 11 – 9, DOI: 10.1016/s0021-9290(97)00104-8.
- [48] J. S. Stroud, S. A. Berger and D. Saloner, Influence of stenosis morphology on flow through severely stenotic vessels: implications for plaque rupture, *Journal of Biomechanics* **33**(4) (2000), 443 – 455, DOI: 10.1016/s0021-9290(99)00207-9.
- [49] P. S. Swaye, L. D. Fisher, P. Litwin, P. A. Vignola, M. P. Judkins, H. G. Kemp, J. G. Mudd and A. J. Gosselin, Aneurysmal coronary artery disease, *Circulation* **67**(1) (1983), 134 – 138, DOI: 10.1161/01.cir.67.1.134.
- [50] G. B. Thurston, Plasma release cell layering theory for blood flow, *Biorheology* **26**(2) (1989), 199 – 214, DOI: 10.3233/BIR-1989-26208.
- [51] G. B. Thurston, Rheological parameters for the viscosity, viscoelasticity and thixotropy of blood, *Biorheology* **16** (1979), 149 – 162, DOI: 10.3233/bir-1979-16303.
- [52] C. Tu and M. Deville, Pulsatile flow of non-Newtonian fluids through arterial stenoses, *Journal of Biomechanics* **29**(7) (1996), 899 – 908, DOI: 10.1016/0021-9290(95)00151-4.

- [53] A. Valencia and M. Villanueva, Unsteady flow and mass transfer in models of stenotic arteries considering fluid-structure interaction, *International Communications in Heat and Mass Transfer* **33** (2006), 966 – 975, DOI: 10.1016/j.icheatmasstransfer.2006.05.006.
- [54] G. R. Zendehebudi and M. S. Moayeri, Comparison of physiological and simple pulsatile flows through stenosed arteries, *Journal of Biomechanics* **32**(9) (1999), 959 – 965, DOI: 10.1016/s0021-9290(99)00053-6.

